AIP Advances

Cavity ring down spectroscopy of cold neutral phenanthrene and phenanthridine in supersonic jets

Cite as: AIP Advances **9**, 085021 (2019); https://doi.org/10.1063/1.5100152
Submitted: 15 April 2019 . Accepted: 05 August 2019 . Published Online: 21 August 2019

Salma Bejaoui, and Farid Salama

Cavity ring down spectroscopy of cold neutral phenanthrene and phenanthridine in supersonic jets

Cite as: AIP Advances 9, 085021 (2019); doi: 10.1063/1.5100152
Submitted: 15 April 2019 • Accepted: 5 August 2019 •
Published Online: 21 August 2019

Salma Bejaoui[1,2,a)] and Farid Salama[1,a)]

AFFILIATIONS

[1] NASA-Ames Research Center, Space Science & Astrobiology Division, Mail Stop 245-6, Moffett Field, California 94035-1000, USA
[2] NPP, Universities Space Research Association, 615 National Ave, Mountain View, California 94043, USA

[a)] Corresponding author: salmabejaoui@gmail.com; farid.salama@nasa.gov

ABSTRACT

Here we study the effect of nitrogen insertion on the electronic spectra of polycyclic aromatic hydrocarbon (PAH) molecules measured under laboratory conditions that are relevant for comparison with astronomical data. We examine the case of the substitution of carbon atoms by nitrogen atoms in the benzenoid skeleton of phenanthrene ($C_{14}H_{10}$), a prototype non-compact PAH. The vibronic transitions of the $2^1A_1(S_1) \longleftarrow X^1A_1(S_0)$ electronic absorption band system of neutral phenanthrene ($C_{14}H_{10}$) and phenanthridine ($C_{13}H_9N$) molecules seeded in a supersonic free jet expansion of argon gas are measured in the 315-345 nm region using the cavity ring down spectroscopy (CRDS) technique. Additional measurements of the absorption spectra of the phenanthrene, phenanthridine, and 1,10-phenanthroline ($C_{12}H_8N_2$) molecules isolated in 10-K solid argon matrices are also presented. The results obtained confirm that laboratory spectra of cold, isolated molecules obtained under astrophysically relevant conditions are required for a direct, unambiguous comparison with astronomical observations as well as for the understanding of the physical evolution of the interstellar medium.

I. INTRODUCTION

Astronomical observations show that large carbon-bearing molecules, such as polycyclic aromatic hydrocarbons (PAHs) and fullerenes are present in the interstellar medium (ISM) of the Milky Way and extragalactic environments. The ubiquitous infrared emission features observed at 3.3, 6.2, 7.7, 8.6, 11.2, and 12.7 μm and attributed to vibrational transitions occurring in PAH ions and molecules are observed in a variety of astrophysical objects in different galaxies galaxies (Leger and Puget, 1984; Allamandola et al., 1985; Smith et al., 2007; Tielens, 2008; Ehrenfreund and Cami, 2010; Boersma et al., 2012; and Lee et al., 2013). PAH molecules are also thought to contribute to the 217.5 nm interstellar extinction bump bump (Witt et al., 1983; Xiang et al., 2011) and have been proposed as plausible carriers of the diffuse interstellar bands (DIBs), a set of hundreds of absorption features seen in the spectra of astronomical objects in the Milky Way and other galaxies in the ultraviolet, visible and infrared wavelengths. The so-called PAH-DIB proposal is based on the expected abundance of PAHs in the ISM and their stability against the photo- and thermo- dissociation (Crawford et al., 1985; Leger and D'Hendecourt, 1985; and Van der Zwet and Allamandola, 1985). Neutral and ionized PAHs exhibit electronic transitions from the near-UV to the near-IR, which depend strongly on the size, the shape, and the ionization state of the molecule. Their absorption features can be broad and strong in the UV/Vis or narrow and weak in the Vis/NIR. This can explain the distribution of DIBs between broad/strong and weak/narrow bands and supports the hypothesis of their potential contribution to the interstellar extinction (Salama, 1999; Salama et al., 2011).

PAHs in the ISM are expected to be present in the gas phase as cold free molecules in various charge states. Extensive laboratory efforts have been underway to study the spectroscopy of PAHs under interstellar-like conditions. Matrix isolation spectroscopy (MIS) has provided an extensive database of the absorption spectra of

neutral and ionized PAHs trapped in Ne or Ar matrices at low temperatures (5-10 K) (see Salama (1999) for a review). However, the shift and the broadening of the spectral bands induced by the solid matrix environment make it impossible to assign specific bands to astronomical observations. Laboratory gas-phase spectra of PAHs have been performed subsequently thanks to the development of the highly-sensitive CRDS technique, which provided a new set of spectroscopic data of neutral and ionized interstellar PAH analogs with sub-ppm sensitivity that can now be compared directly with astronomical observation (Biennier et al., 2003; Tan and Salama, 2005a; 2005b; Staicu et al., 2006; and Rouillé et al., 2007).

Despite the extensive theoretical and experimental effort, no DIB features have yet been definitively assigned to the spectral signature of a specific PAH. A pool of neutral and ionized organics (unsaturated hydrocarbons, PAHs, and fullerenes) has been proposed by Salama (1998) as the best correlation that matches the DIBs features. In 1994, two DIBs detected at 963.2 and 957.7 nm were suggested to be associated with the absorption of C_{60} + molecules in Ne matrix (Fulara et al., 1993; Foing and Ehrenfreund, 1994). This assignment was confirmed recently by laboratory measurements of gas phase C_{60} + (Campbell et al., 2015; Walker et al., 2016). This recent achievement has motivated new astronomical searches as well as additional experimental studies to enhance the laboratory interstellar PAH analogs database, especially in the NUV -to- NIR range where the electronic absorption spectral bands are measured and can be used to unambiguously identify the signature of specific PAH molecules and ions in the ISM. Moreover, more astronomical observations of DIBs with better signal to noise ratio and higher resolution are required in the ranges that have not been frequently observed (NUV and NIR). Efforts are ongoing in this direction as well with new extensive DIB surveys (e.g., The European Southern Observatory Diffuse Interstellar Band Large Exploration Survey (EDIBLES), (Cox et al., 2017)).

The interstellar PAH population is thought to include a wide distribution of related molecular species, i.e., regular PAHs in various charge states (neutral and ions), PAHs with multiple shapes and structures (compact and non-compact), PAH derivatives with aliphatic side groups attached to their benzenoid rings, as well as PAHs with carbon atoms substituted by heteroatoms. Recent infrared spectroscopy studies have suggested that nitrogen-substituted PAHs (PANHs) could also be abundant in the interstellar environment as nitrogen is one of the most abundant after hydrogen, helium, and carbon (Spitzer, 1978). PANHs exhibit spectral features similar to PAHs and may contribute as well to the observed unidentified interstellar bands (Mattioda et al., 2003; Bernstein et al., 2005; Mattioda et al., 2005; and Alvaro Galué et al., 2010). Theoretical researches studying the effect of substitution of C – H bond(s) by a nitrogen atom(s) in PAHs on the C – C stretching mode proposed that large endoskeletal PAHs (i.e the N-atom substitution occurs in the internal site of the aromatic structure) reproduce better the 6.2 μ m infrared emission band (Peeters et al., 2002). This band has attracted particular interest because the emission band of PAH cations in this region is red-shifted compared to the astronomical data and various PAH-related species have been proposed to explain this shift (larger PAH sizes, PANH cations, closed-shell cationic PAHs, and aliphatic groups). While IR spectroscopy supports the case of the possible presence of PANHs in the ISM and their contribution to the UIRs, very few studies have targeted their electronic spectroscopy in the gas phase. Here, we attempt to address the lack of information regarding PAHs and PANHs electronic spectroscopy and we present a comparative study of the absorption spectra of neutral phenanthrene ($C_{14}H_{10}$, hereafter Phen) and phenanthridine ($C_{13}H_9N$, hereafter PhenN) seeded in supersonic jets of argon and measured with cavity ring down spectroscopy (CRDS). The experimental setups, COSmIC for the gas-phase CRDS experiments and the MIS setup are briefly described in section II. The results obtained in the gas phase are presented and compared with spectra obtained in solid inert-gas (argon or neon) matrices in section III.

II. EXPERIMENTAL

A. Cavity ring down spectroscopy (CRDS)

The experimental setup, COSmIC, standing for cosmic simulation chamber, has been described in detail previously (Biennier et al., 2003; Tan and Salama, 2005a; and 2005b) (figure 1). Briefly,

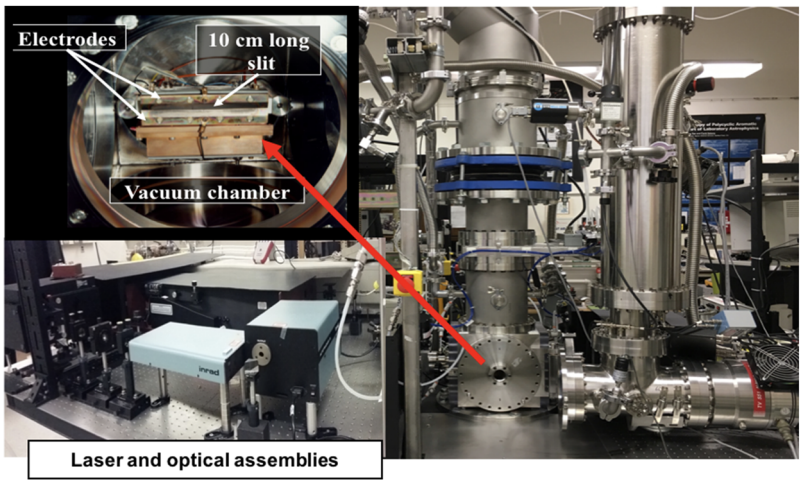

FIG. 1. Experimental setup: Cosmic simulation chamber coupled to the cavity ring down spectrometer.

the apparatus combines a pulsed discharge slit nozzle (PDN) with a cavity ring-down spectrometer for high-sensitivity absorption measurements. The PDN consists of a heated copper reservoir with a 10 cm × 127 μm slit mounted in a vacuum chamber. Two synchronized pulsed solenoid valves (General Valve Series 9) are inserted inside the reservoir to drive a Vespel slit poppet (Dupont, SP-22 Grade) that opens and seals the slit from the inside. Phen and PhenN samples (Sigma Aldrich, 98%) are introduced at the bottom of the reservoir and heated up to 120 °C to increase their concentrations in the expansion. The argon carrier gas is injected into the PDN, mixes with the PAH vapor and expands through the rectangular slit in 1280 μs-long pulses and generates a 10 Hz pulsed collision-free planar expansion.

Cavity ring-down spectra of Phen and PhenN are recorded at 2 mm downstream the slit nozzle where the measured rotational temperature is of the order of 52 K (Tan and Salama, 2005a). The backing pressure of Ar is 592 Torr while the background pressure in the vacuum chamber is maintained at 75 mTorr by a mechanical booster pump with a capacity of 250 l/s. The supersonic jet is probed using laser excitation tuned over the 315-340 nm range (29412 to 31 746 cm^{-1}) with a spectral bandwidth of 0.2 cm^{-1}. The tunable laser pulses are generated with a Nd:YAG (Quanta-Ray Lab 150 from Spectra-Physics) pumped dye laser (Quanta-Ray PDL-2 from Spectra-Physics) using a mixture of DCM and LDS 698 dyes (Exciton). The output of the dye laser is frequency doubled by an angle-tuned BBO crystal (Type 'TSS', in an Autotracker III (Inrad)) and the fundamental and doubled wavelengths are separated by a four-prism beam separator. The UV laser is spatially filtered using a 1:1 telescope equipped with a 20 μ m pinhole aperture. The CRD spectra are recorded by scanning the dye laser with an increment of 0.012 nm. A pair of high-reflectivity (HR) mirrors (Layertec, HR (0°, 325-360 nm) ≥99.9%) are mounted on both sides of the chamber 62 cm apart. Each of the two mirrors is fixed on a mount with three micrometer-screws for fine-tuning alignment. The ring-down signal is detected with a photodetector (H6780-04 from Hamamatsu) and monitored with a Tektronix TDS3052 oscilloscope. The data are then processed by a PC program and the cavity losses are extracted. Wavelength calibration is achieved externally by recording the laser wavelengths simultaneously along with the CRD spectra.

B. Matrix isolation spectroscopy (MIS)

The MIS experimental setup has been described in detail previously (Salama and Allamandola, 1991; Salama et al., 1994). Briefly, the MIS apparatus consists of a cubic chamber maintained under high vacuum ($P < 10^{-8}$ torr) with a combination of diffusion and mechanical pumps. The chamber is equipped with four ports and two gas injection inlets at 45° angles with respect to the ports. A sample holder suspended at the center of the chamber is cooled down to 6 K by a closed-cycle helium cooled cryostat (APD Cryogenics, Inc. model HC-2). The temperature of the substrate is measured with a Fe-Au/Chrome1 thermocouple connected to the sample holder. The samples are vaporized from a heated Pyrex finger valve while argon is admitted through a flowmeter connected to an adjacent tube. The vapor pressures of Phen and PhenN are of the order of 0.2 and 0.1 mtorr at room temperature (Oja and Suuberg, 1998), a pressure high enough for the preparation of the argon-matrices samples without the need of applying external heating. Absorption spectra are measured using a deuterium lamp (Oriel corporation) that provides a smooth continuum from 160 to 360 nm. After passing through the sample, the light is collimated into an optical fiber using a spherical lens (f=150 mm) and guided to the entrance slit of a monochromator (IsoPlane SCT 320, Princeton Instruments) with a focal length of 320 mm and an aperture ratio f/4.6. A grating with a groove density of 600/mm blazed at 600 nm combined with an entrance slit of 5 μ m provide a spectral resolution of about 0.015 nm. The detector is a 1024 × 1024 pixels intensified charge-coupled device (ICCD) area array (Gen II PI-MAX, Princeton Instruments) thermoelectrically cooled down to −20 °C. The camera and the spectrograph are monitored using commercially supplied software (Winspec, Princeton Instruments). The reference spectrum (spectrum of the deuterium lamp before the PAH deposition), the dark spectrum (spectrum recorded when the light source is off) and the sample spectra (spectra of the matrices recorded at several depositions time) are recorded using the same detection parameter (integration time, average). Finally, the wavelength calibration of the spectrometer is provided by the emission lines of a mercury lamp.

III. RESULTS AND DISCUSSION

A. Absorption spectrum of phenanthrene ($C_{14}H_{10}$)

The absorption spectrum of Phen seeded in a supersonic jet of Ar was previously measured in our laboratory and reported in Salama et al. (2011). In that subsequent paper, the spectrum was calibrated using two weak and broad bands of He I produced in the plasma at 318.77 and 323.13 nm. In this study, the CRD spectrum is recorded simultaneously with the detection of the laser wavelength using an external spectrograph. The comparison between the two CRD spectra show identical band shapes and peak positions which validate our calibration technique. Figure 2 shows the CRD absorption of Phen in the gas phase (solid line) compared to the MIS spectra of Phen measured in both solid neon and argon matrices at 6 K and 10 K, respectively (dashed and dotted lines). The MIS spectrum in neon matrix was measured by Salama et al. (1994) using an open cycle liquid helium transfer cryostat. The MIS measurements in Ne and Ar matrices shown in figure 2 were arbitrarily blue-shifted for comparison with the gas phase spectrum. The results show a good agreement between the absorption measurements in the gas and solid phases and highlight the spectral perturbations that are induced by the lattice environment in the solid inert-gas matrices in terms of band-peak positions, band profiles and band broadening. This effect is particularly apparent in the case of the Ar matrix. The comparison clearly illustrates the need of gas phase measurements for more accurate comparisons with astronomical spectra.

The full CRD spectrum of Phen was recorded twice and the spectral absorption features were analyzed separately. The comparison between the two sets of measurements shows high repeatability with an error in peak positions less than 0.05 nm. A large number of vibronic bands (74 in total) were observed in the 315-345 nm (28985 to 31 746 cm^{-1}) spectral range. This region is associated with the Singlet band system I: $2^1A_1(S_1) \longleftarrow X^1A_1(S_0)$ electronic

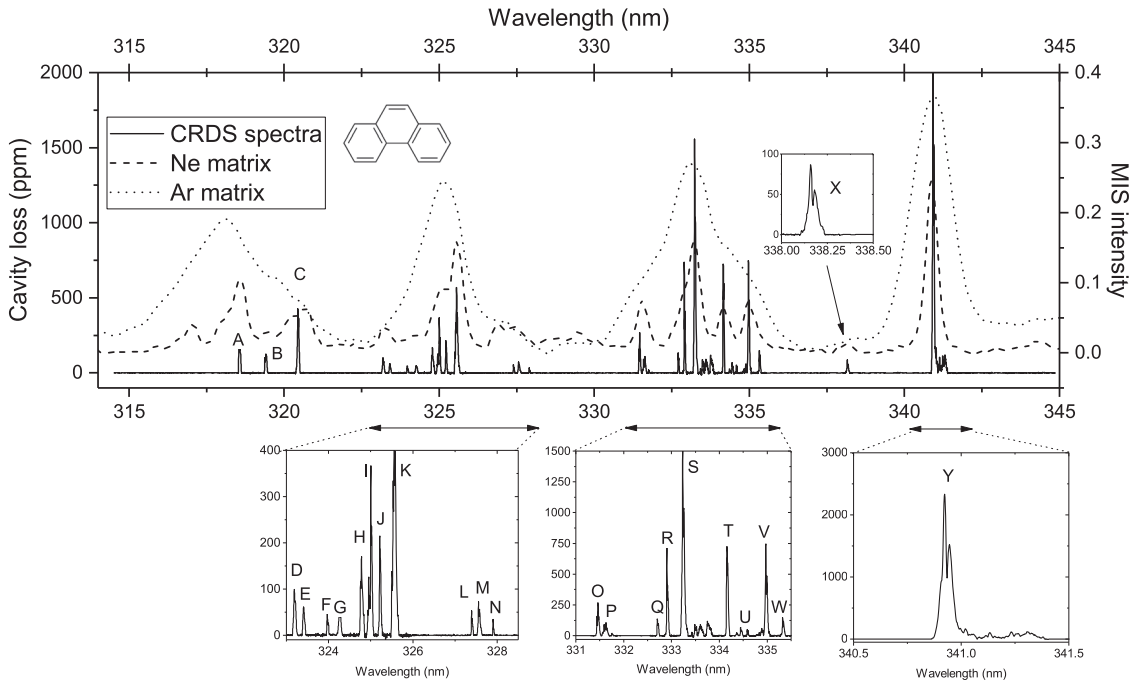

FIG. 2. The absorption spectrum of gas-phase phenanthrene ($C_{14}H_{10}$) seeded in an Ar supersonic jet expansion (solid line) is compared with the absorption spectrum of phenanthrene embedded in solid Ne (dashed line from Salama et al. (1994)) and solid Ar (dotted line) matrices. Blue shifts of 0.2 nm and 2.4 nm have been applied to the Ne and Ar matrix spectra, respectively for comparison with the gas phase spectrum.

transition (Salama et al., 1994). The peak position, the full width at half maximum (FWHM) for each vibronic band fitted with Lorentzian profile, and the relative absorption intensity (H/H_{max}) are listed in Table I. The features observed in the CRD spectrum of jet-cooled Phen are assigned by comparison with the fluorescence excitation spectrum measured by Kowaka et al. (2012) in a jet cooled Ar gas and to their *ab initio* theoretical calculation using GAUSSIAN 09 program package (Kowaka et al., 2012). In the CRD spectrum, the strongest band in the $S_1 \longleftarrow S_0$ system peaks at 29 332 cm^{-1} (340.92 nm ∓ 0.05 nm) and corresponds to the transitions observed at 29 324 cm^{-1} (341.02 nm) and 29 316 cm^{-1} (341.11 nm) in the fluorescence excitation and Ne matrix spectra, respectively. The red-shift between the absorption band positions in Ne matrix and the CRD spectra is between 15 and 30 cm^{-1}. A shift of the same order is observed when comparing the CRD absorption spectrum with the fluorescence excitation spectrum. The absorption bands reported here exhibit a higher spectral resolution and the fluorescence excitation transitions represent the convolution of two or more vibronic absorption bands. The broadening and the slight shift (~7-21 cm^{-1}) in band peak positions might be due to the different temperature in the two supersonic expansion measurements (the rotational temperature (T_{rot}) of Phen is estimated at 12 K in Kowaka et al. (2012) study while T_{rot} is of the order of 52 K in our supersonic expansion (Tan and Salama, 2005a)). Finally, the FWHM values of the bands observed in the CRD spectrum range from 1.09 to 33 cm^{-1} (0.009 to 0.15 nm). We note that these values are consistent with the FWHM observed for the narrow DIBs that range from 0.04 to 4 nm (Salama, 2001).

B. Absorption spectrum of phenanthridine ($C_{13}H_9N$)

The cavity ring-down spectroscopy of PhenN was conducted under the same experimental conditions as for Phen (i.e., using the same carrier gas (Ar), the same backing pressure (592 Torr) and the same heating temperature for the PAH reservoir (120 °C)). The fluorescence excitation and the fluorescence spectra of PhenN cooled in Helium jet expansion have been reported by Prochorow et al. (2004). However, to the best of our knowledge, no absorption measurements have been reported in the literature for this molecule in either the solid or gas phases.

We present in figure 3 the absorption spectra of PhenN measured using the CRDS (solid line) and the MIS (dotted line) techniques. In this figure, the spectrum of PhenN isolated in Ar matrix (at 10 K) is arbitrarily blue-shifted for comparison with the gas phase spectrum in the cooled jet. We report in Table II the Lorentzian-fitted positions and the FWHM of the absorption bands of the CRD spectrum. The absorption band positions are compared to the fluorescence excitation features reported by Prochorow et al. (2004) and to the MIS results. The bands observed in the 315-340 nm (29412 to 31 746 cm^{-1}) spectral range are also associated with the Singlet band system I: $2^1A_1(S_1) \longleftarrow X^1A_1(S_0)$ vibronic transition. The strongest

TABLE I. Vibronic transitions of neutral phenanthrene ($C_{14}H_{10}$) seeded in an Ar free jet expansion (CRDS) compared to the fluorescence excitation spectra in jet-cooled Ar reported by Kowaka et al. (2012) and the absorption of Phen isolated in solid matrices of Ne (Salama et al., 1994). $\Delta\nu^* = \nu - \nu_{CRDS}$.

	CRDS measurements				Fluorescence excitation			Ne matrix	
	λ nm	ν cm^{-1}	FWHM cm^{-1}	H/H_{max} %	ν cm^{-1}	$\Delta\nu^*$ cm^{-1}	Assignment	ν cm^{-1}	$\Delta\nu^*$ cm^{-1}
	341.31	29298.96	1.5	5.1					
	341.26	29302.91	2.3	3.8					
	341.23	29305.46	2.0	4.8					
	341.13	29314.02	1.6	4.5					
	341.06	29320.68	4.0	3.1					
Y	341.02	29323.77	2.0	7.1					
	341.00	29325.90	1.2	7.4					
	340.98	29327.45	2.2	11.8					
	340.95	29330.17	2.4	65.3					
	340.92	29332.15	1.6	100.0	29324	8.1	0_0^0	29316.9	15.2
	340.91	29333.48	2.3	40.2					
	338.18	29569.79	2.6	2.4					
X	338.16	29571.84	1.4	3.7	29562	9.8	$23_0^1(a_1)$	29550.8	21.0
	335.34	29820.64	2.2	5.1					
W	335.32	29822.07	1.3	6.4	29808	14.1	$65_0^1(b_2)$		
	334.99	29851.30	3.3	20.6				29832.94	18.4
V	334.97	29853.31	1.4	32.0	29840	13.3	$21_0^1(a_1)$		
	334.60	29886.40	1.4	1.8					
U	334.58	29887.95	1.0	2.2					
	334.45	29900.24	1.6	2.9					
	334.17	29924.52	2.0	24.7					
T	334.16	29925.79	1.8	31.1	29913	12.8	$64_0^1(b_2)$	29904.3	21.5
	333.26	30006.90	4.5	44.4	29992	14.9	-		
S	333.23	30008.93	1.6	66.8	29996	12.9	$20_0^1(a_1)$	29994.0	14.9
	332.92	30037.39	1.9	17.5					
R	332.90	30038.80	1.4	31.6	30025	13.8	$63_0^1(b_2)$		
	332.72	30055.06	2.9	4.2					
Q	332.71	30056.64	2.4	5.7	30049	7.6	-		
	331.77	30141.48	3.0	0.4					
	331.76	30142.72	2.2	0.8					
	331.67	30150.72	2.0	1.3					
P	331.65	30152.56	2.2	2.7	30143	9.6	$19_0^1(a_1)$		
	331.62	30155.36	3.4	2.5					
	331.59	30157.62	2.0	3.9					
	331.57	30159.11	1.3	1.3					
	331.48	30167.86	1.2	6.7					
O	331.46	30169.23	1.4	11.4	30153	16.2	$62_0^1(b_2)$	30138.6	30.6
	327.92	30495.44	2.2	0.6					
N	327.90	30496.66	1.5	1.4	30479	17.7	$15_0^1(a_1)$		
	327.58	30526.75	1.9	2.4					
M	327.56	30528.88	1.9	3.1	30512	16.9	$58_0^1(b_2)$		
	327.41	30542.88	1.5	1.5					
L	327.39	30544.17	1.7	2.3					

TABLE I. (*Continued.*)

	CRDS measurements				Fluorescence excitation			Ne matrix	
	λ nm	ν cm^{-1}	FWHM cm^{-1}	H/H_{max} %	ν cm^{-1}	$\Delta\nu*$ cm^{-1}	Assignment	ν cm^{-1}	$\Delta\nu*$ cm^{-1}
K	325.65	30707.64	3.4	1.8					
	325.61	30711.40	5.4	5.1					
	325.60	30712.24	2.7	9.0					
	325.58	30714.33	3.1	17.1					
	325.53	30718.75	2.8	14.4					
	325.51	30721.41	2.7	5.9					
J	325.21	30748.92	1.9	9.2	30729	19.9	-		
I	325.02	30767.22	3.2	10.0					
	325.00	30768.91	2.0	15.7	30752	16.9	$54_0^1(b_2)$	30740.8	28.1
	324.97	30771.62	1.5	3.7					
	324.95	30773.60	1.5	5.4					
	324.94	30775.35	2.3	2.3					
H	324.78	30789.88	2.8	7.3	30773	16.9	$10_0^1(a_1)$		
	324.76	30791.97	3.9	4.9					
G	324.28	30837.19	4.2	1.7					
F	324.26	30839.56	6.6	2.0	30825	14.6	-		
E	324.00	30864.67	4.2	1.1	30848	16.7	$52_0^1(b_2)$		
	323.97	30867.00	4.1	2.0	30852	15.0	-		
	323.41	30920.51	6.0	2.6	30902	18.5	$7_0^1(a_1)$		
D	323.21	30939.51	5.1	3.1					
	323.19	30941.69	4.1	4.2	30921	20.7	$50_0^1(b_2)$	30921.5	20.2
C	320.47	31204.62	3.2	15.7					
	320.44	31206.70	2.3	18.2				31172.5	34.2
B	319.43	31305.66	5.4	4.9					
	319.41	31307.43	3.6	5.4	31293	14.4	-		
	319.38	31310.26	3.8	4.4					
A	318.60	31387.74	3.5	5.5					
	318.58	31389.26	2.6	6.7					
	318.56	31391.05	2.1	12.1	31374	17.0	-	31377.7	13.4
	318.54	31392.80	3.9	10.6					

band in this system peaks at 29 608.7 cm^{-1} (337.74 nm) and corresponds to the transition observed at 29 611 cm^{-1} (337.71 nm) in the fluorescence excitation spectrum and 29 364.15 cm^{-1} (340.8 nm) in the Ar matrix. The FWHM values of the bands observed in the CRDS spectra range from 0.9 to 16 cm^{-1} while broader bands are observed in the Ar matrix spectrum (120 to 5000 cm^{-1}). A good agreement in the band positions is found between the CRD and the fluorescence excitation transitions obtained by Prochorow et al. (2004). A small shift (<4 cm^{-1}) is observed in some structures where the fluorescence excitation bands correspond to the convolution of two or more vibronic absorption transitions. The CRD spectrum obtained in this study has narrower and more resolved features compared to the fluorescence excitation bands, which can be explained by a difference of PhenN temperature in the expansions. The Doppler broadening effect enhanced for the axisymetric nozzle jet in the Prochorow et al. (2004) study where the velocity dispersion is higher compared to planar expansion may contribute to the difference in the spectral resolution as well (Lovejoy and Nesbitt, 1987).

C. Effect of nitrogen insertion in the benzenoid skeleton

The substitution of C-H bond with N atom reduces the symmetry of phenanthrene and induces non-bonding electrons (a pair of electrons in the valence shell of each N atom) which affects the geometry of the molecule. Deperasinska et al. (2004) show in their theoretical study that the lengths of the PhenN chemical bonds and the angles between the adjacent bonds are different compared to the parent molecule in both ground and excited singlet states.

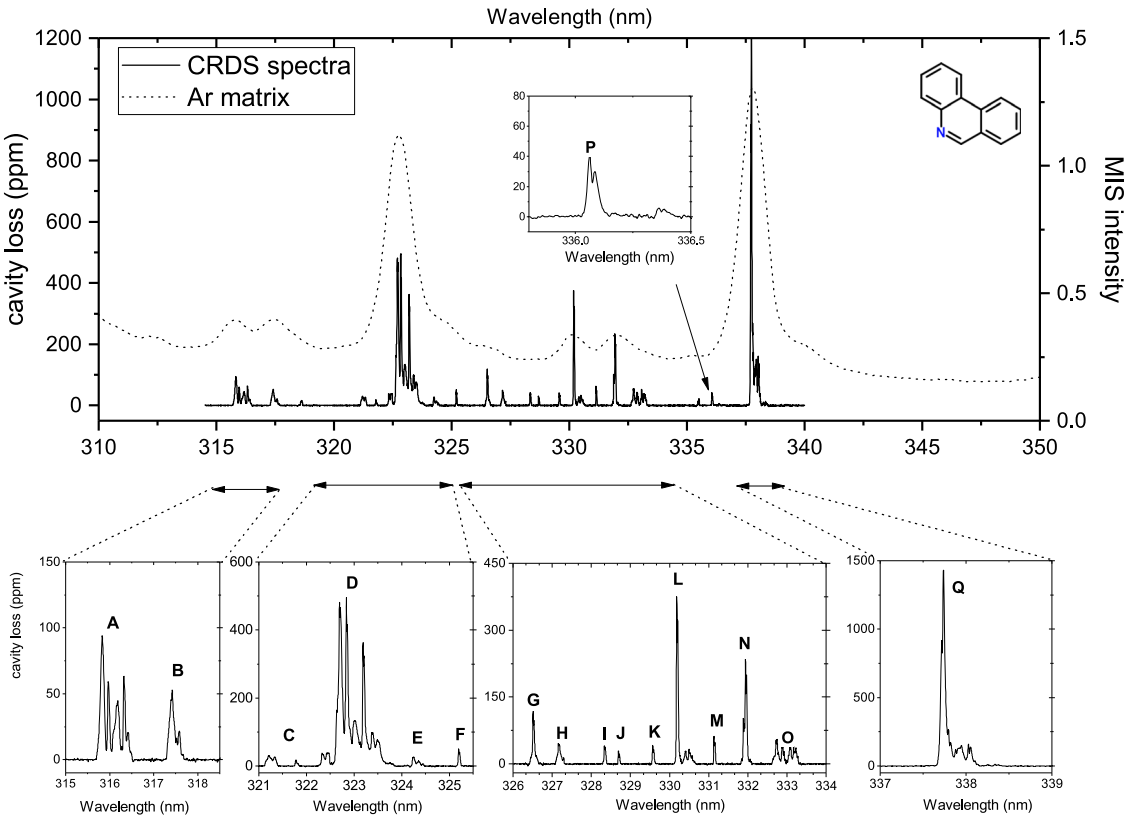

FIG. 3. The absorption spectrum of gas-phase phenanthridine ($C_{13}H_9N$) seeded in Ar supersonic jet expansion (solid line) is compared with the absorption spectrum of phenanthridine embedded in solid Ar matrix (dotted line). A blue-shift of 2.8 nm has been applied to the MIS spectrum for comparison with the gas phase spectrum.

This deformation doesn't only affect the ring where the N atom is introduced but extends to the other aromatic rings. The lower symmetry and the deformation of the benzenoid skeleton of N-substituted PAH have a direct impact on the electronic and vibronic transitions. The PhenN spectrum obtained in the present study exhibits more absorption transition (106 bands) compared to Phen (74 bands). Similar result has been observed in the study of Prochorow et al. (2004) where the vibrational activity of molecules increased from phenanthrene to phenanthridine to 7,8-benzoquinoline (N atom inserted in the external ring). The increased number of rovibronic transitions is due to favorable Franck-Condon factors that enable additional non-totally symmetric planar vibrations, which were prohibited in Phen molecules (Deperasinska et al., 2004). Additionally, the absorption spectrum of PhenN is blue-shifted compared to Phen and the two strongest bands of both molecules are shifted by 277 cm^{-1} to higher energies (figure 4). A close comparison between the band profiles of these two bands shows similar bandwidths (see insert plot in figure 4). No broadening induced by the insertion of one nitrogen in the skeleton has been observed in the S_1 system of PhenN.

To further probe the effects of the insertion of additional nitrogen atoms in the PAH skeleton, we measured and compared the absorption spectra of Phen, PhenN and 1,10-phenanthroline ($C_{12}H_8N_2$, PhenNN) isolated in Ar matrices (see figure 5). In all these measurements, the deposition of the sample was performed at room temperature. The full spectra were recorded after 30 min of deposition while the inserted plot associated with the weaker band systems corresponds to 3h deposition. The spectra presented in figure 5 (30 min and 3h of deposition) are normalized to their highest band intensity.

As can be seen in figure 5, the PhenN has broader absorption bands compared to Phen below 300 nm where the electronic transitions occur from S_0 ground state to the excited singlet states S_i, $i \geq 2$. PhenNN molecules exhibit two strong bands in the 200-300 nm region. The first structure at short wavelengths is the strongest one and can be deconvolved into two narrow bands at 223.8 and 228.3 nm, respectively similar to the $(S_5) \longleftarrow (S_0)$ system observed in the spectrum of Phen (Salama et al., 1994). The second feature in the 235-300 nm region, also strong, peaks at 260.9 nm and exhibits a very broad structure. At the longer wavelength (>300 nm), Phen, PhenN and PhenNN all have very weak band systems, especially in the case of PhenNN (insert plot in figure 5). While Phen has 5 bands with the same order of magnitude in the S_1 system, PhenN exhibits only 2 strong and 3 weaker structures and PhenNN has 2

TABLE II. Vibronic transitions of neutral phenanthridine ($C_{13}H_9N$) in gas phase (CRDS) seeded in an Ar free jet expansion compared to the fluorescence excitation spectrum in jet-cooled Helium reported by Prochorow et al. (2004) and the absorption of PhenN in Ar matrix.

	CRDS measurements				Fluorescence excitation	MIS measurements	
	λ nm	ν cm^{-1}	FWHM cm^{-1}	H/H_{max} %	ν cm^{-1}	ν cm^{-1}	FWHM cm^{-1}
					29391		
	338.19	29568.80	1.42	0.3			
	338.13	29574.41	3.45	0.9			
	338.10	29576.74	3.14	2.6			
	338.05	29581.11	3.35	9.6			
	338.03	29583.31	1.39	11.3			
	338.01	29584.81	2.15	4.3			
	337.96	29589.17	3.20	7.1			
	337.95	29590.49	4.77	10.5			
	337.92	29592.41	0.92	9.2			
	337.91	29593.96	3.68	9.0			
	337.88	29596.32	2.49	8.4			
	337.82	29601.59	3.75	12.1			
	337.79	29603.83	2.97	18.8			
	337.74	29608.73	2.43	100.0	29611	29364.1	126.4
	337.72	29610.55	3.38	64.4			
	336.38	29727.91	2.23	0.3			
P	336.36	29729.86	3.65	0.0			
	336.08	29754.38	3.54	2.1	29756		
	336.06	29756.31	2.39	2.9			
	333.28	30005.03	5.73	1.1			
	333.23	30009.34	1.38	2.4	30009		
	333.17	30014.40	2.05	2.6			
	333.10	30021.33	5.11	2.5			
	333.07	30023.35	1.51	3.6	30023		
O	333.04	30026.29	2.48	1.3			
	332.92	30036.98	2.52	1.8			
	332.89	30039.75	3.44	2.7	30042		
	332.87	30041.32	3.24	2.8			
	332.78	30049.78	3.03	1.6			
	332.74	30053.07	3.50	3.7	30055		
	332.72	30054.98	2.90	3.5			
	331.97	30123.63	4.70	13.9			
	331.94	30125.79	2.51	16.4	30127	29869.0	158.0
N	331.91	30128.50	2.15	6.2			
	331.89	30130.67	3.20	7.1	30131		
	331.85	30134.53	3.02	0.8			
M	331.16	30197.10	4.89	3.5	30200		
	331.14	30199.06	2.52	4.5			
	330.57	30250.36	3.92	1.1			
	330.52	30255.49	6.62	1.5			
	330.50	30257.42	3.10	2.2			
	330.43	30263.59	6.21	0.8			
L	330.41	30265.04	3.98	1.9			
	330.40	30266.22	2.56	1.9			
	330.29	30276.42	2.26	0.8			
	330.27	30278.66	3.87	1.2			
	330.21	30284.06	3.85	22.9	30286	30030.4	143.0
	330.19	30285.99	2.39	14.5			

TABLE II. (*Continued.*)

	CRDS measurements				Fluorescence excitation	MIS measurements	
	λ nm	ν cm^{-1}	FWHM cm^{-1}	H/H_{max} %	ν cm^{-1}	ν cm^{-1}	FWHM cm^{-1}
K	329.59	30340.34	3.81	2.3	30342		
	329.57	30342.59	2.45	3.0			
J	328.72	30421.17	3.22	1.8	30422		
	328.69	30423.42	2.41	2.3			
I	328.35	30454.97	5.42	2.8			
	328.34	30456.62	2.80	3.0			
H	327.18	30564.03	4.85	3.0			
	327.16	30565.87	3.07	3.6			
G	326.53	30624.73	3.42	6.8	30624		
	326.51	30626.59	3.63	8.3			
F	325.22	30748.85	3.53	2.9	30749		
	325.20	30750.59	2.49	3.6			
E	324.25	30840.16	4.35	1.8			
	324.23	30841.88	2.73	1.8			
D	323.39	30922.20	6.50	6.5			
	323.37	30923.96	3.47	6.5			
	323.34	30927.22	2.72	3.2			
	323.29	30932.23	8.43	4.2			
	323.26	30935.15	3.54	5.7			
	323.21	30939.77	4.53	22.5	30939		
	323.19	30941.57	2.98	25.5			
	323.13	30947.57	2.60	4.6			
	323.08	30951.63	4.46	5.5			
	322.91	30968.42	3.52	7.5			
	322.86	30973.45	4.64	28.9	30973		
	322.84	30975.18	2.57	35.0			
	322.71	30987.23	3.21	32.5	30988		
	322.69	30989.09	3.33	33.8		30719.6	153.2
	322.66	30992.61	4.47	13.8			
	322.64	30994.69	4.35	11.2			
	322.57	31001.41	2.40	0.4			
	322.52	31005.51	1.85	0.3			
	322.45	31012.73	1.90	2.4			
	322.43	31014.95	3.87	2.3			
	322.37	31019.85	9.03	1.3			
	322.37	31019.97	1.36	2.0			
	322.33	31024.30	3.47	2.4	31021		
C	321.33	31120.38	10.29	1.8			
	321.29	31124.22	3.56	1.5			
	321.21	31132.09	16.06	2.1			
	321.11	31141.78	4.20	1.1			
B	317.42	31504.08	3.81	3.7			

TABLE II. (*Continued.*)

	CRDS measurements				Fluorescence excitation	MIS measurements	
	λ nm	ν cm^{-1}	FWHM cm^{-1}	H/H_{max} %	ν cm^{-1}	ν cm^{-1}	FWHM cm^{-1}
	316.34	31611.78	7.04	3.7			
	316.32	31613.50	3.57	4.7		31234.3	230.3
	316.28	31618.02	1.77	0.5			
	316.21	31624.62	3.78	2.2			
	316.19	31627.05	4.37	3.0			
	316.15	31630.14	2.94	2.7			
	316.13	31633.00	8.03	1.6			
A	316.10	31635.81	6.00	1.3			
	316.08	31637.96	3.72	1.1			
	315.98	31647.74	5.49	3.5			
	315.96	31649.11	3.92	4.1			
	315.83	31662.61	3.04	6.4		31387.1	164.1
	315.78	31667.98	3.40	3.8			
	315.77	31668.37	3.52	2.1			
	315.75	31670.89	3.72	0.9			
						31770.2	268.2
						32085.9	166.6
						32652.1	298.1
						32820.7	427.2
						34026.7	929.0
						34346.9	258.0
						35186.5	279.1
						35590.6	277.2
						36645.9	713.0
						37331.4	1036.4
						39901.1	2481.9
						41984.3	1314.5
						42459.9	5176.6

strong and 3 weaker bands. Finally, the lowest-energy transition system of PhenN is blue shifted by 3 nm compared to Phen while a larger blue-shift of 13 nm is observed in the case of PhenNN. The spectral broadening observed for PhenN and notably for PhenNN molecules could be explained by the overlapping of a large number of electronic and rovibronic transitions unresolved due to the perturbation of the solid matrix effect. The insertion of a second N atom deforms more the molecule and increases further its vibrational

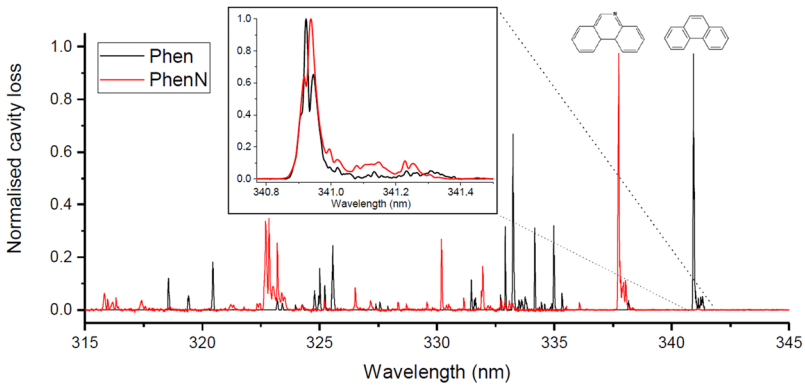

FIG. 4. CRD spectra of phenanthrene ($C_{14}H_{10}$, black) and phenanthridine ($C_{13}H_9N$, red) seeded in Ar supersonic jets. The strongest band in the S_1 system of PhenN is red-shifted by 3.2 nm (277 cm^{-1}) in the insert plot for comparison with that associated with Phen.

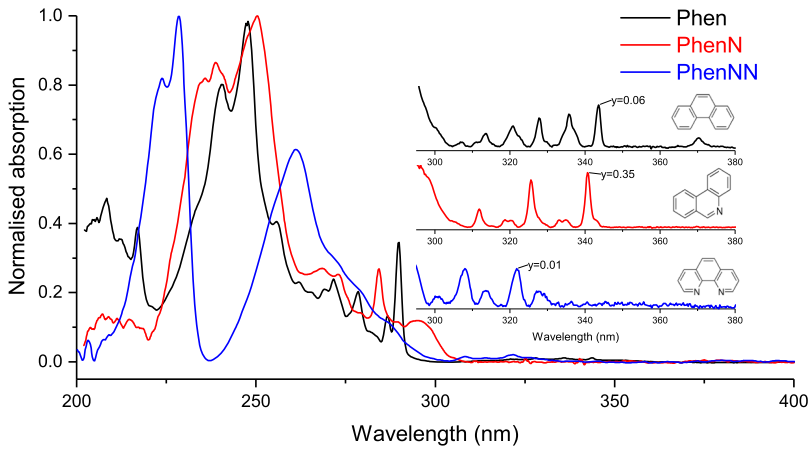

FIG. 5. Absorption spectra of phenanthrene ($C_{14}H_{10}$, black), phenanthridine ($C_{13}H_9N$, red) and 1,10-phenanthroline ($C_{12}H_8N_2$, blue) isolated in Ar matrices at 10 K. The full-range spectra correspond to 30 min deposition. The spectra shown in the 280-380 nm range in the insert plots for the weaker bands correspond to 3h of deposition.

activity consistently with Deperasinska et al. (2004). Gas phase measurements with shortest wavelengths are required to confirm this conclusion.

IV. CONCLUSION

In this work, we report the first measurements of the gas phase spectra of neutral phenanthridine ($C_{13}H_9N$) in the 315-345 nm region that we compare to new measurements of the gas phase spectra of neutral phenanthrene ($C_{14}H_{10}$). The absorption spectra were measured using the cavity ring-down technique by intercepting a tunable laser with a pulsed supersonic expansion jet of argon seeded with PAH (or PANH). Additional measurements of the absorption spectra of phenanthrene, phenanthridine, and 1,10-phenanthroline ($C_{12}H_8N_2$) isolated in argon and neon matrices are also reported. The main conclusions of this study are summarized as follows:

(1) The comparison between CRDS and MIS spectra highlights the broadening and the redshift of the band peak positions that are induced by interaction with the phonons of the solid matrix and points out to the need for gas phase measurements for more accurate comparisons with astronomical data.

(2) Good agreements have been obtained between the CRD absorption spectra and the fluorescence excitation spectroscopy results measured by Kowaka et al. (2012) and Prochorow et al. (2004) for Phen and PhenN, respectively. The small shift in band positions could be explained by slightly different PhenN temperature in the two jet expansions and by larger Doppler broadening effects induced by the shape of the nozzles (an axisymetric nozzle jet) compared to the planar expansion in our experiments.

(3) The substitution of C-H bonds with nitrogen atoms in the benzenoid skeleton of the PAH molecules has a significant impact on the electronic signature of these molecules. The deformation and the reduction of the molecule's symmetries increase the number of rovibronic transitions and blueshift the lowest-energy transition of the PhenN S_1 system by 3 nm compared to the parent molecule. A larger blueshift of 13 nm is obtained between Phen and PhenNN isolated in argon matrices.

ACKNOWLEDGMENTS

Funding for this work was provided by the NASA SMD APRA Program. S.B acknowledges the support of the NASA Postdoctoral Program (NPP). The authors also acknowledge fruitful discussions with C.S. Contreras and L. Biennier and the outstanding technical support of R. Walker and E. Quigley.

REFERENCES

Allamandola, L. J., Tielens, A. G. G. M., and Barker, J. R., Astrophys. J. Lett. **290**, L25 (1985).
Alvaro Galué, H., Pirali, O., and Oomens, J., Astron. Astrophys. **517**, A15 (2010).
Bernstein, M. P., Sandford, S. A., and Allamandola, L. J., "The mid-infrared absorption spectra of neutral polycyclic aromatic hydrocarbons in conditions relevant to dense interstellar clouds," Astrophys. J. Sup. Ser. **161**(1), 53 (2005).
Biennier, L., Salama, F., Allamandola, L. J., and Scherer, J. J., "Pulsed discharge nozzle cavity ringdown spectroscopy of cold polycyclic aromatic hydrocarbon ions," J. Chem. Phys. **118**(17), 7863 (2003).
Boersma, C., Rubin, R. H., and Allamandola, L. J., Astrophys. J. **753**(2), 168 (2012).
Campbell, E. K., Holz, M., Gerlich, D., and Maier, J. P., Nature **523**, 322 (2015).
Cox, N. L. J. *et al.*, "The ESO diffuse interstellar bands large exploration survey (edibles)—I. Project description survey sample, and quality assessment," Astron. Astrophys. **606**, A76 (2017).
Crawford, M. K., Tielens, A. G. G. M., and Allamandola, L. J., Astrophys. J. Sup. Ser. **293**, L45 (1985).
Deperasinska, I., Prochorow, J., and Stepanenko, Y., Acta Phys. Pol. A **106**(4), 535–545 (2004).
Ehrenfreund, P. and Cami, J., Cold Spring Harb. Perspect. Biol. **2**(12), a002097 (2010).
Foing, B. H. and Ehrenfreund, P., Nature **369**(6478), 296 (1994).
Fulara, J., Jakobi, M., and Maier, J. P., Chem. Phys. Lett. **211**(2), 227 (1993).
Kowaka, Y., Yamanaka, T., and Baba, M., J. Chem. Phys. **136**(15), 154301 (2012).
Lee, N. *et al.*, Astrophys. J. **778**, 131 (2013).
Leger, A. and D'Hendecourt, L., Astron. Astrophys. **146**, 81 (1985).
Leger, A. and Puget, J. L., Astron. Astrophys. **137**, L5 (1984).
Lovejoy, C. M. and Nesbitt, D. J., Rev. Sci. Instrum. **58**(5), 807 (1987).
Mattioda, A., Hudgins, D., Bauschlicher, C., and Allamandola, L., "Infrared spectroscopy of matrix-isolated polycyclic aromatic compounds and their ions. 7. Phenazine, a dual substituted polycyclic aromatic nitrogen heterocycle," Adv. Space Res. **36**(2), 156 (2005).
Mattioda, A. L., Hudgins, D. M., Bauschlicher, C. W., Rosi, M., and Allamandola, L. J., J. Phys. Chem. A **107**(10), 1486 (2003).
Oja, V. and Suuberg, E. M., J. Chem. Eng. Data **43**(3), 486 (1998).

Peeters, E., Hony, S., Van Kerckhoven, C., Tielens, A. G. G. M., Allamandola, L. J., Hudgins, D. M., and Bauschlicher, C. W., Astron. Astrophys. **390**(3), 1089 (2002).

Prochorow, J., Deperasińska, I., and Stepanenko, Y., Chem. Phys. Lett. **399**, 239 (2004).

Rouillé, G., Arold, M., Staicu, A., Krasnokutski, S., Huisken, F., Henning, T., Tan, X., and Salama, F., J. Chem. Phys. **126**(17), 174311 (2007).

Salama, F., *Origins of Life and Evolution of the Biosphere* (Kluwer Academic Publishers, 1998), volume 28.

Salama, F., Solid Interstellar Matter: The ISO Revolution **65** (1999).

Salama, F., J. Mol. Struct. **563-564**, 19 (2001).

Salama, F. and Allamandola, L. J., J. Chem. Phys. **94**(11), 6964 (1991).

Salama, F., Galazutdinov, G. A., Krełowski, J., Biennier, L., Beletsky, Y., and Song, I.-O., Astrophys. J. **728**(2), 154 (2011).

Salama, F., Joblin, C., and Allamandola, L. J., J. Chem. Phys. **101**(12), 10252 (1994).

Smith, J.-D. T. *et al.*, Astron. J. **656**, 770 (2007).

Spitzer, L., Physical processes in the interstellar medium (1978).

Staicu, A., Krasnokutski, S., Rouillé, G., Henning, T., and Huisken, F., J. Mol. Struct. **786**, 105 (2006).

Tan, X. and Salama, F., "Cavity ring-down spectroscopy and theoretical calculations of the $S_1(^1B_{3u})$-$S_0(^1A_g)$ transition of jet-cooled perylene," J. Chem. Phys. **122**, 084318 (2005a).

Tan, X. and Salama, F., "Cavity ring-down spectroscopy and vibronic activity of benzo[ghi]perylene," J. Chem. Phys. **123**(1), 014312 (2005b).

Tielens, A., Annu. Rev. Astron. Astrophys. **46**(1), 289 (2008).

Van der Zwet, G. P. and Allamandola, L. J., Astron. Astrophys. **146**, 76 (1985).

Walker, G. A. H., Campbell, E. K., Maier, J. P., Bohlender, D., and Malo, L., Astrophys. J. **831**(2), 130 (2016).

Witt, A. N., Bohlin, R. C., and Stecher, T. P., Astrophys. J. Sup. Lett. **267**, L47 (1983).

Xiang, F. Y., Li, A., and Zhong, J. X., Astrophys. J. **733**(2), 91 (2011).